PNAS
www.pnas.org

Supplementary Information for

Volumetric and shear processes in crystalline rock approaching faulting

François Renard, Jessica McBeck, Neelima Kandula, Benoît Cordonnier, Paul Meakin, and Yehuda Ben-Zion

Corresponding author: François Renard
Email: francois.renard@geo.uio.no

This PDF file includes:

Text: Strain measurements
Table S1
Figs. S1 to S2
Captions for movies S1 to S2

Other supplementary materials for this manuscript include the following:

Movies S1 to S2

www.pnas.org/cgi/doi/10.1073/pnas.1902994116

Table S1: List of symbols and parameters used in the Figures 4 and S2

Symbol	Description and unit
σ_1	axial stress (MPa)
$\sigma_3 = \sigma_2$	confining pressure (MPa)
$\sigma_D = (\sigma_1 - \sigma_3)$	differential stress (MPa)
σ_D^f	differential stress at failure (MPa)
$\Delta\sigma_D = \sigma_D^f - \sigma_D$	differential stress at failure minus differential stress (MPa)
$\Delta_D = (\sigma_D^f - \sigma_D)/\sigma_D^f$	stress control parameter that measures the distance to failure (without unit)
φ	void fraction (i.e. porosity) of the sample (without unit)
φ_i	initial porosity before deformation (without unit)
D_φ	damage volume fraction equal to $\frac{\varphi-\varphi_i}{1-\varphi_i}$ (without unit)
n_f	number of microfractures that open during a stress step
α, β	exponents of power laws (Figure 4)
$\nabla\cdot\Delta\mathbf{u}$	divergence of the incremental displacement field calculated using digital volume correlation, used as a proxy of the volumetric strain
$\nabla\times\Delta\mathbf{u}$	curl of the incremental displacement field calculated using digital volume correlation, used as a proxy of the shear strain
$\varepsilon_{zz}^M, \varepsilon_r^M$	macroscopic axial and radial strains (without unit)
Δ_n	node spacing in the digital volume correlation calculation (m)
d	incremental shear displacement calculated using the digital volume correlation calculation (m)
δv^+	positive (microfracture opening) volume increment (m^3)
δv^-	negative (microfracture closing) volume increment (m^3)
$\Sigma\delta v$	total microfracture volume increase in the sample at a given state of differential stress, corresponding to $\Sigma\delta v = \lvert\Sigma\delta v^+\rvert - \lvert\Sigma\delta v^-\rvert$ (δv^- is a negative volume change)
V	volume of the sample (m^3)

Text: Strain measurements

Strain in the sample was measured by using three complementary techniques. Measuring the specimen dimensions during deformation from the tomograms quantified macroscopic radial and axial strain (Figs. 2A, SI Appendix, Fig. S1 and Movie S1). We quantified strain heterogeneities in the sample in situ by: 1) calculating three-dimensional displacements fields via digital volume correlation (Figs. 2C-D, 3, SI Appendix, Movie S2); and 2) segmenting the microfractures from the host rock to track the evolving volume of microfractures (Figs. 2A, 2B, 4, SI Appendix, Fig. S2 and Movie S1). The macroscopic axial strain, ε_{zz}^{M}, was calculated from the distance between the two pistons visible in the tomograms inset in SI Appendix, Fig. S1). We verified that the axial strain was equal to the displacement of the piston measured using a displacement sensor installed on the rig, after correction for the deformation of the rig and the pistons (SI Appendix, Fig. S1). The macroscopic radial strain, ε_{r}^{M}, was determined by measuring the diameter of the sample at six different positions on each tomogram and by calculating the average value (SI Appendix, Fig. S1). The macroscopic volumetric strain at the onset of failure, $(\varepsilon_{zz}^{M} + 2\varepsilon_{r}^{M})$, was equal to 2.1%, and the volume fraction of microfractures was 1.4%. The difference between these two quantities is attributed primarily to the presence of microfractures with apertures below the resolution of the X-ray tomography images. The volumes of pre-existing microfractures and other voids present before the differential stress was applied must have changed during the experiment, as the non-linear strain-stress relationship and relatively small effective Young's modulus at differential stresses less than 40 MPa suggests. However, the volumetric strain was very small until yielding commenced at a differential stress of 178 MPa, and this implies that pre-existing voids contributed little to the volumetric strain at the onset of failure.

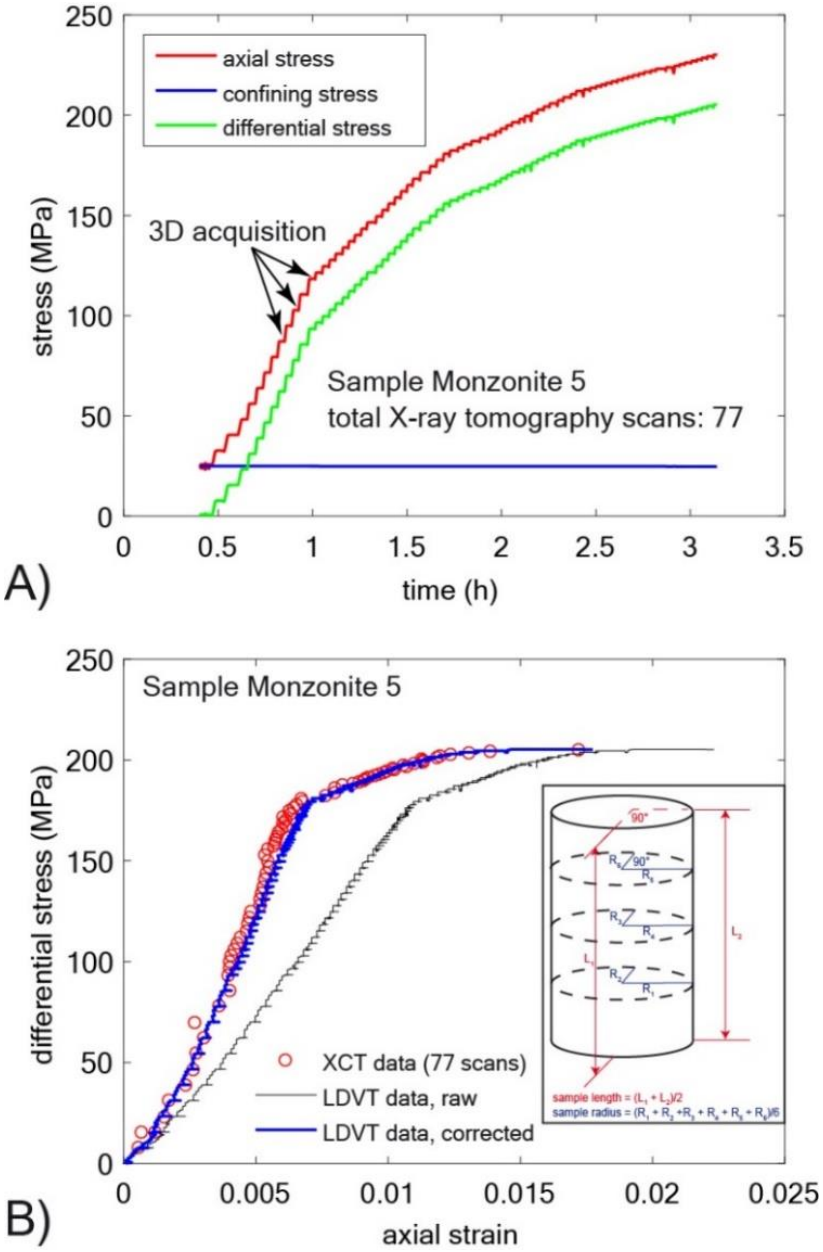

Fig. S1. Stress history and strain measurements. A) Stress history during deformation of the quartz-rich monzonite sample. The top of each step in the axial stress curve corresponds to one of the 77 X-ray tomography acquisitions. B) Comparison of measurement of the axial strain by using: 1) direct measurement of the shortening of the specimen using three-dimensional images (red circles); and 2) the linear variable differential transformer (LVDT) displacement sensor (black curve) installed on the Hades rig (Renard et al., 2016). The LDVT measurements were corrected to account for the elastic deformation of the rig and the pistons (blue curve). Inset: Procedure used to measure the average length and radius of the core sample (the radius was measured in two mutually perpendicular directions within three planes perpendicular to the axial direction).

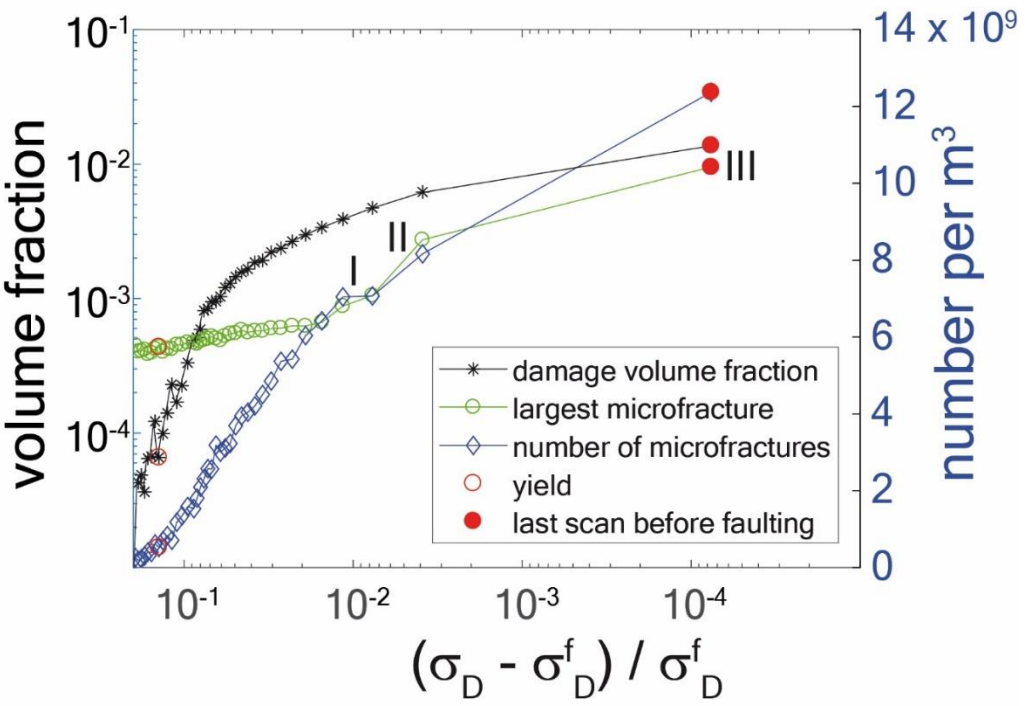

Fig. S2. Microfracture volume evolution prior to failure in crystalline rock. Evolution of the damage volume fraction (i.e. volume of microfractures divided by volume of the sample), number of microfractures per cubic meter and volume fraction of the largest microfracture cluster as failure was approached (σ_D^f: differential stress at failure). The numbers I, II, III correspond to the three differential stresses at which the views of the largest microfracture cluster are shown in the inset of Fig. 2A.

Movie S1. Deformation of the specimen and damage development prior to failure. Left: three-dimensional rendered view of the specimen with the rock matrix shown in gray shades and the microfracture porosity shown in blue. Top right: differential stress versus axial and radial strains. The open red circle shows the yield point and the full red circle shows the stress at failure. Bottom right: Mohr diagram throughout loading. The thick black line shows the Coulomb failure criterion using a cohesion of 49.7 MPa and internal friction of 0.6, which were estimated from the data and from the deformation of two other samples determined in a previous study (Renard et al., 2018).

Movie S2. Spatial distribution of positive and negative divergence and positive and negative curl magnitudes above the 95th percentile of each incremental strain population normalized by the incremental macroscopic axial strain difference, $\Delta\varepsilon_{zz}^{M}$, between the successive pairs of tomograms used to determine the incremental strain population. A-D) The diameters of the spheres are proportional to the magnitudes of $\boldsymbol{\nabla} \cdot \Delta\boldsymbol{u}$ and $\boldsymbol{\nabla} \times \Delta\boldsymbol{u}$, which were calculated at the digital volume correlation analysis nodes. A) Gray spheres show the negative divergence (compaction); B) blue spheres show positive divergence (dilation); C) pink spheres show negative curl, and D) red spheres show positive curl. E) Axial strain versus differential stress with vertical lines showing the differential stress and axial strain of the pair of tomograms used to determine the incremental displacement fields by DVC analysis. Sum (F), mean (G), and number of values (H) within population of incremental strain calculated from digital volume correlation analysis. F-H) The values are normalized by the value of the first digital volume correlation increment of the experiment, and shown as a function of the macroscopic axial strain at which the second scan used in the digital volume correlation analysis was acquired.

References

1. Renard F, et al. (2016) A deformation rig for synchrotron microtomography studies of geomaterials under conditions down to 10 km depth in the Earth. *Journal of Synchrotron Radiation* 23:1030-1034.

2. Renard F, et al. (2018) Critical evolution of damage toward system-size failure in crystalline rock. *Journal of Geophysical Research: Solid Earth* 123. https://doi.org/10.1002/2017JB014964.